Available online at www.sciencedirect.com
SCIENCE DIRECT®
Journal of Sound and Vibration 268 (2003) 779–797
JOURNAL OF SOUND AND VIBRATION
www.elsevier.com/locate/jsvi

Spectral finite elements for vibrating rods and beams with random field properties

M. Ostoja-Starzewski[a,*], A. Woods[b,1]

[a] Department of Mechanical Engineering, McGill University, Montreal, Que. Canada H3A 2K6
[b] Allstate Insurance Co., Northbrook, IL 60062, USA

Received 22 February 2001; accepted 24 November 2002

Abstract

The classical stochastic Helmholtz equation grasps, through the random field of the refraction index, the spatial variability in the mass density but not the variability in elastic moduli or geometric parameters. In contradistinction to this restriction, the present analysis accounts for the spatial randomness of mass density as well as those of elastic properties and cross-sectional geometric properties of rods undergoing longitudinal vibrations and of Timoshenko beams in flexural vibrations. All the material variabilities are described here by random Fourier series with a typical (average) characteristic size of inhomogeneity d, which is either smaller, comparable to, or larger than the wavelength. The third length scale entering the problem, but kept constant, is the rod or beam length. We investigate the relative effects of random noises in all the material parameters on the spectral stiffness matrices associated with rods and beams for a very wide range of frequencies.

1. Introduction

1.1. Background

Dynamics of any structure involves wave propagation in all the members of the structure. Therefore, a structural dynamics analysis should be based on the governing elastodynamic equations. This is best accomplished by a so-called spectral approach. In it, the response of each and every structural member is described by a stiffness matrix in the frequency space which is appropriately called a *spectral finite element*. The classical static stiffness matrix is actually

*Corresponding author. Tel.: +514-398-7394; fax: +514-398-7365.
E-mail address: martin.ostoja@mcgill.ca (M. Ostoja-Starzewski).
[1] Formerly at Department of Mathematical Sciences, Northern Illinois University, DeKalb, IL 60115, USA.

0022-460X/03/$ - see front matter © 2003 Elsevier Science Ltd. All rights reserved.
doi:10.1016/S0022-460X(03)00037-3

obtained from the spectral stiffness matrix in a zero-frequency limit. By connecting all the elements according to the spatial geometry, a global stiffness matrix is constructed and a global response due to a specified impulse is studied first by going over all the frequencies and then by transforming to the time domain, which is conveniently done by the fast Fourier transform (FFT); see, for example, Ref. [1].

The overwhelming majority of natural as well as man-made materials are characterized by the presence of imperfect microstructures. This introduces a length scale d, the typical size of inhomogeneity, in addition to the two scales (the typical wavelength λ and the element size L) already present in the classical formulation. As a result, the spectral matrix of any given finite element should reflect an interplay of three length scales: the element size L, the typical wavelength λ, and the typical size of inhomogeneity d.

Let us note here that the classical stochastic Helmholtz equation (e.g., Refs. [2,3])

$$\nabla^2 u + k_0^2 n^2(\mathbf{x}, \omega) u = f(\mathbf{x}), \quad \omega \in \Omega, \tag{1}$$

grasps, through the random field of refraction index, the spatial variability in the mass density but not the variability in elastic modulus or cross-section. This is immediately seen by considering the equation governing axial motions in a rod with the space dependent mass density ρ, elastic modulus E, and cross-sectional area A, namely

$$\frac{\partial}{\partial x}\left[A(x,\omega)E(x,\omega)\frac{\partial}{\partial x}u(x,t)\right] = \rho(x,\omega)A(x,\omega)\frac{\partial^2}{\partial t^2}u(x,t), \quad \omega \in \Omega. \tag{2}$$

In the above, ω denotes an element of the sample space Ω. Thus, $\rho(x,\omega)$ stands for one realization of the random field of density $\rho = \{\rho(x,\omega); x \in X, \omega \in \Omega\}$ over a domain X, and similarly with E and A.

In contradistinction to the restriction implicit in Eq. (1), the analysis reported here accounts for the spatial variabilities of mass density as well as those of elastic properties and cross-sectional geometric properties of a rod governed by Eq. (2). In effect, we conduct a study of the imperfection sensitivity of the spectral stiffness matrices, whereby the characteristic size of inhomogeneity—either in E, or ρ, or A—varies from $d < \lambda$ through $d > \lambda$. This study constitutes the first part of the paper. First, for completeness, in Section 2, we derive a simpler form of the spectral finite element for the Helmholtz equation than ever reported before. Then, in Section 3, we turn to the stochastic problem, and set up a numerical method for solving Eq. (2) in the frequency domain whereby the material and geometric properties of the rod are modelled as random Fourier series. Section 4 contains a discussion of the results of our parameter studies with a focus on the k_{11} coefficient of the spectral matrix.

In the second part, in an analogous fashion, we consider dynamics of Timoshenko beams with spatially random properties

$$\frac{\partial}{\partial x}\left[GA\kappa\left(\frac{\partial v}{\partial x} - \phi\right)\right] = \frac{\partial^2 v}{\partial t^2},$$

$$\frac{\partial}{\partial x}\left[EI\frac{\partial \phi}{\partial x}\right] + GA\kappa\left(\frac{\partial v}{\partial x} - \phi\right) + \rho I\omega^2\phi = \frac{\partial^2 \phi}{\partial t^2}. \tag{3}$$

It is well known that there are two kinds of wave motion in such a beam: flexural and rotational. We focus on the first of these so as to keep the results to manageable proportions. The spatial inhomogeneity is modelled again by random Fourier series, although it now involves five (rather than three) independent parameters appearing in the governing equations: mass density ρ, elastic modulus E, the Poisson ratio v, area A and moment of inertia I of the cross-section. It is more physical, however, to work with the cross-sectional height h and cross-sectional width w instead of the latter two. Thus, the beam is described by a five component random field $[\rho, E, v, h, w]$. Given the need to conduct our study by computational methods, we can focus on select aspects of the problem at hand. Thus, we choose to analyze the imperfection sensitivity of the coefficient k_{11} in the spectral matrix; this coefficient relates the transverse displacement to the shear force at one end of the beam. And we do so when the characteristic size of inhomogeneity in E, v, ρ, h, or w varies from $d < \lambda$ through $d > \lambda$. In Section 5, we review the spectral finite element for the deterministic Timoshenko beam. In Section 6, we set up the stochastic Timoshenko beam equations and then set up a numerical method for solving them in the frequency domain when all or only some of the material and geometric properties of the beam are random. Section 7 contains a discussion of numerical results. The paper concludes in Section 8.

Our research has been motivated by a need to better understand the elastodynamics of paper and concrete, two materials which are well known to possess random, multiscale structures. The particular numbers we choose below for material parameters of rods and beams correspond to concrete.

2. Spectral finite element for 1-D wave motion in a homogeneous rod

The elastodynamic equation governing the axial response of a rod (assuming zero external forcing) is well known

$$\frac{\partial^2 u}{\partial x^2} = \frac{1}{c_a^2}\frac{\partial^2 u}{\partial t^2}. \tag{4}$$

Here $c_a = \sqrt{E/\rho}$ denotes the phase velocity of axial waves; E being the elastic axial modulus and ρ the mass density.

Let us now consider harmonic motions according to $u(x,t) = \hat{u}(x)e^{i\gamma t}$, γ being the frequency. Then, the spectral matrix expresses a connection between the kinematic and the dynamic quantities—i.e., $\{\hat{u}_1, \hat{u}_2\}$ with $\{\hat{F}_1, \hat{F}_2\}$—at both ends of the rod: 1 and 2. The hat signifies that the quantities are in the frequency space. The derivation of the spectral stiffness matrix is carried out as follows. For the Helmholtz equation corresponding to the 1-D wave equation (4) set up over the domain X of size L,

$$\frac{d^2\hat{u}}{dx^2} + k^2\hat{u} = 0, \quad u(0) = \hat{u}_1, \quad u(L) = \hat{u}_2, \tag{5}$$

with $k = \gamma/c_a$, we consider a solution in the form

$$\hat{u}(\xi) = A\sin k\xi + B\sin k(L-\xi). \tag{6}$$

From the boundary conditions $(5)_{2,3}$ we immediately get $A = \hat{u}_2/\sin kL$ and $B = \hat{u}_1/\sin kL$, so that Eq. (5) becomes

$$\hat{u}(\xi) = \frac{\hat{u}_1 \sin k(L-\xi) + \hat{u}_2 \sin k\xi}{\sin kL}. \tag{7}$$

Differentiating with respect to ξ, we find a force along ξ as

$$\hat{F}(\xi) = AE\frac{-\hat{u}_1 k \cos k(L-\xi) + \hat{u}_2 k \cos k\xi}{\sin kL}, \tag{8}$$

which, with the definitions $\hat{F}_1 = -\hat{F}(0)$ and $\hat{F}_2 = \hat{F}(L)$, yields the spectral matrix

$$\begin{bmatrix} \hat{F}_1 \\ \hat{F}_2 \end{bmatrix} = AE \begin{bmatrix} k\cot kL & -k\csc kL \\ -k\csc kL & k\cot kL \end{bmatrix} \begin{bmatrix} \hat{u}_1 \\ \hat{u}_2 \end{bmatrix}. \tag{9}$$

Note that this representation of the spectral matrix is more compact than the representation found in Ref. [1] since, in Eq. (9), the purely real nature of the matrix is apparent. The 11-component of this matrix is plotted in Figs. 1–3 parts (a), in black, as the reference case. (See Ref. [1] for the 12-component.) The peaks of $k\cot kL$ in these figures represent the resonant frequencies of the system with $A = 10^{-4}$ m, $E = 27.4$ GPa and $\rho = 2400$ kg/m^3—this corresponds to a rod made of concrete. It is the change from this 'crisp' functional form which is of interest to us in the random media case.

3. Spectral finite element for 1-D wave motion in an inhomogeneous rod

We now consider a frequency space version of the stochastic equation (2) with Dirichlet boundary conditions

$$\frac{\mathrm{d}}{\mathrm{d}x}\left[A(x,\omega)E(x,\omega)\frac{\mathrm{d}\hat{u}}{\mathrm{d}x}\right] + \rho(x,\omega)A(x,\omega)\hat{u}(x) = 0, \quad \omega \in \Omega,$$

$$\hat{u}(0) = \hat{u}_1, \quad \hat{u}(1) = \hat{u}_2. \tag{10}$$

There are many ways to model imperfect microstructures (e.g., Ref. [4]), and some choices have to be made in the case of beams which themselves are one-dimensional models of three-dimensional bodies. Here we assume the mass density, elastic modulus, and cross-sectional area to vary as

$$A(x,\omega) = A_0\left[1 + \varepsilon_A \sum_{i=1}^{10} \left(a_A^{(i)}(\omega)\cos igx + b_A^{(i)}(\omega)\sin igx\right)\right],$$

$$\rho(x,\omega) = \rho_0\left[1 + \varepsilon_\rho \sum_{i=1}^{10} \left(a_\rho^{(i)}(\omega)\cos igx + b_\rho^{(i)}(\omega)\sin igx\right)\right],$$

$$E(x,\omega) = E_0\left[1 + \varepsilon_E \sum_{i=1}^{10} \left(a_E^{(i)}(\omega)\cos igx + b_E^{(i)}(\omega)\sin igx\right)\right], \tag{11}$$

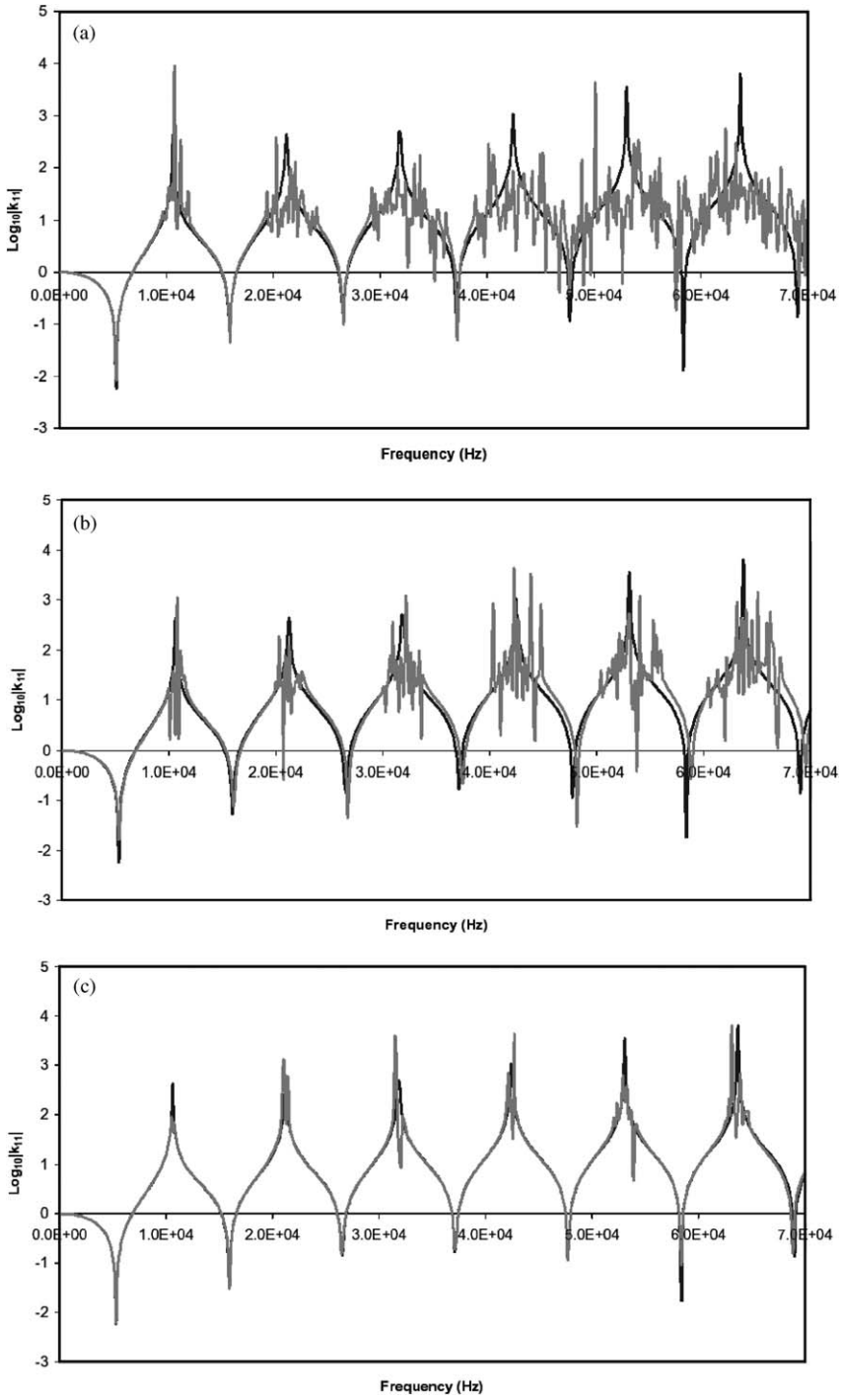

Fig. 1. Rod vibrations in the case of random density ρ showing k_{11} (black line) for the reference homogeneous medium and $\langle k_{11} \rangle$ (grey line) for the random case with: (a) $g = 0.1$, (b) $g = 1.0$, (c) $g = 10.0$.

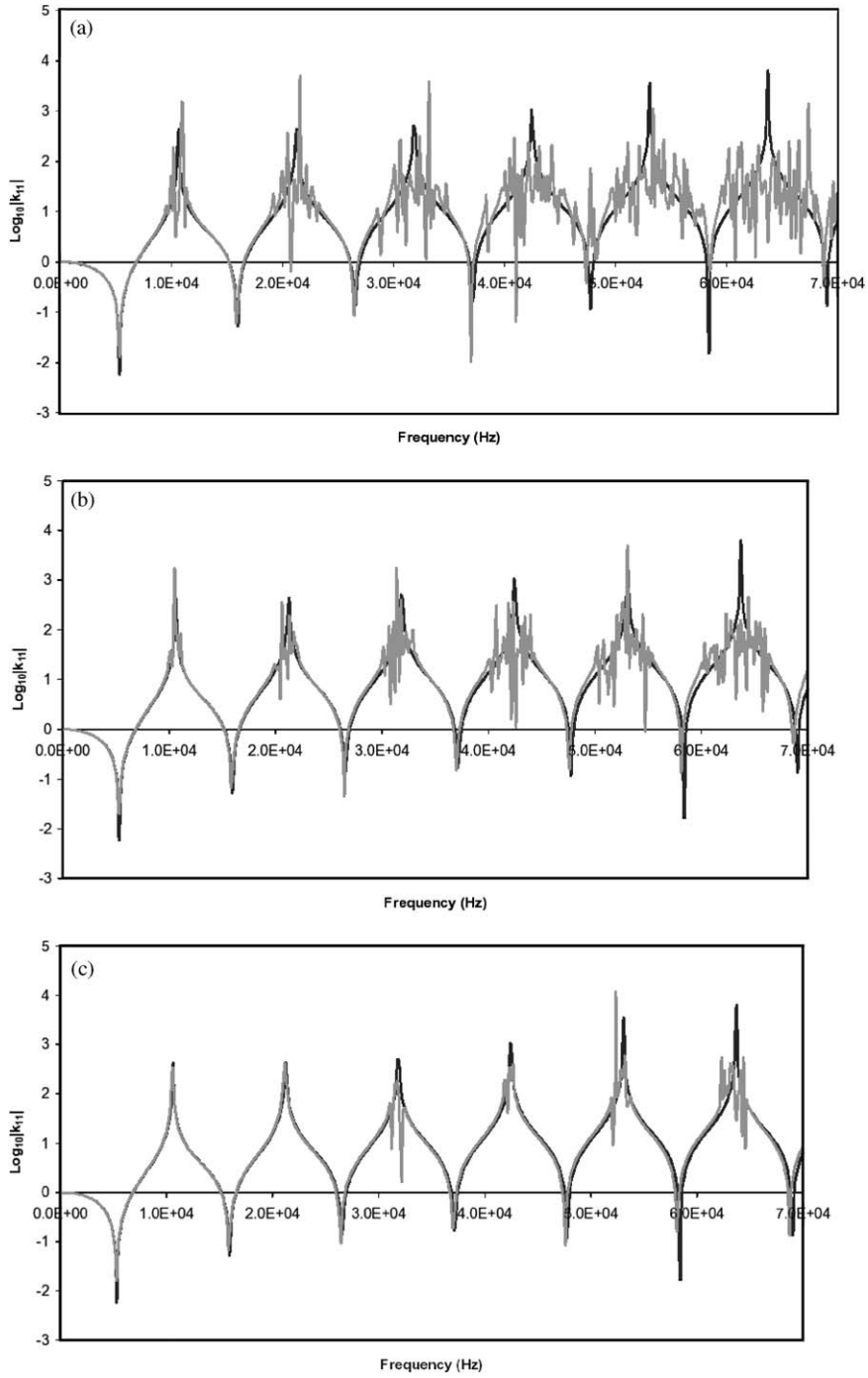

Fig. 2. Rod vibrations in the case of random modulus E showing k_{11} (black line) for the reference homogeneous medium and $\langle k_{11} \rangle$ (grey line) for the random case with: (a) $g = 0.1$, (b) $g = 1.0$, (c) $g = 10.0$.

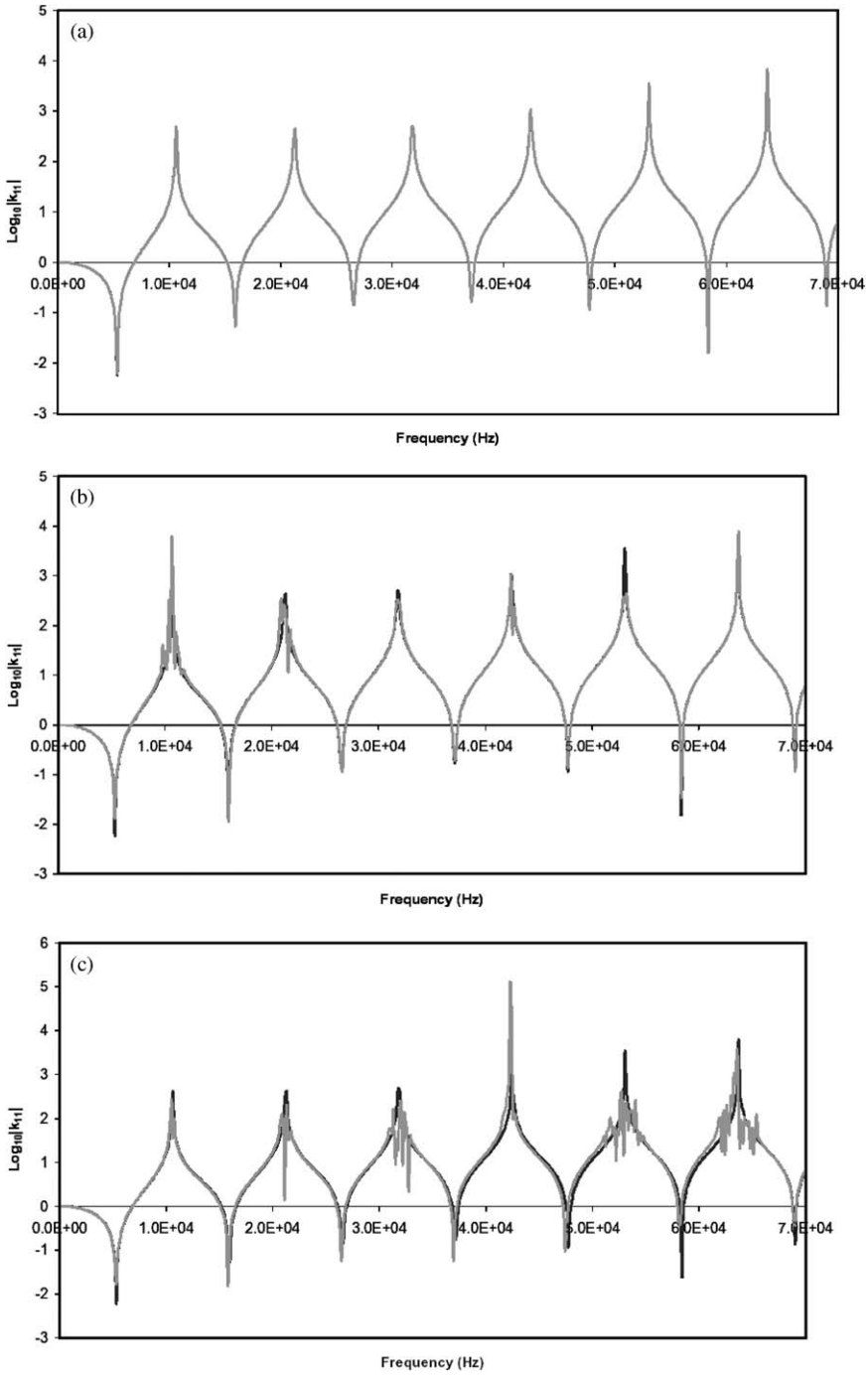

Fig. 3. Rod vibrations in the case of random cross-sectional area A showing k_{11} (black line) for the reference homogeneous medium and mean $\langle k_{11} \rangle$ (grey line) for the random case with: (a) $g = 0.1$, (b) $g = 1.0$, (c) $g = 10.0$.

where for $i = 1, \ldots, 10$, $a_A^{(i)}(\omega), \ldots, b_E^{(i)}(\omega)$ come from a uniform distribution on $[-\frac{1}{2}, \frac{1}{2}]$ and $\omega \in \Omega$. The purpose of this model is not to approximate some "nice" function, but rather, to have a random process model of band-limited type.

We determine the relation

$$\begin{bmatrix} \hat{F}_1 \\ \hat{F}_2 \end{bmatrix} = \begin{bmatrix} k_{11} & k_{12} \\ k_{21} & k_{22} \end{bmatrix} \begin{bmatrix} \hat{u}_1 \\ \hat{u}_2 \end{bmatrix}, \tag{12}$$

as follows. First, for each $g = 0.1, 1$, and 10, we employ a boundary value problem solver [5] to numerically solve Eq. (10) with the following sets of boundary conditions:

$$\begin{gathered} \hat{u}_1(0) = 0.0, \quad \hat{u}_1(1) = 0.0, \\ \hat{u}_2(0) = 0.001, \quad \hat{u}_2(1) = 0.0, \\ \hat{u}_3(0) = 0.0, \quad \hat{u}_3(1) = 0.001, \\ \hat{u}_4(0) = 0.001, \quad \hat{u}_4(1) = 0.001, \\ \hat{u}_5(0) = 0.0005, \quad \hat{u}_5(1) = 0.0005. \end{gathered} \tag{13}$$

Now, since $\hat{F}(x) = AE\hat{u}'(x)$ and the boundary value problem solver generates the values of $\hat{u}'$ at each of the mesh points as part of the numerical solution we may simply calculate the forces at the ends of the rod. They are given by

$$\hat{F}(0) = -AE\hat{u}'(0) \quad \text{and} \quad \hat{F}(1) = AE\hat{u}'(1). \tag{14}$$

Thus, the five sets of boundary conditions in Eqs. (13) lead to the following over-determined linear systems:

$$\begin{bmatrix} \hat{u}_1(0) & \hat{u}_1(1) \\ \hat{u}_2(0) & \hat{u}_2(1) \\ \hat{u}_3(0) & \hat{u}_3(1) \\ \hat{u}_4(0) & \hat{u}_4(1) \\ \hat{u}_5(0) & \hat{u}_5(1) \end{bmatrix} \begin{bmatrix} C_{11} \\ C_{12} \end{bmatrix} = \begin{bmatrix} \hat{F}_1(0) \\ \hat{F}_2(0) \\ \hat{F}_3(0) \\ \hat{F}_4(0) \\ \hat{F}_5(0) \end{bmatrix}, \tag{15}$$

and

$$\begin{bmatrix} \hat{u}_1(0) & \hat{u}_1(1) \\ \hat{u}_2(0) & \hat{u}_2(1) \\ \hat{u}_3(0) & \hat{u}_3(1) \\ \hat{u}_4(0) & \hat{u}_4(1) \\ \hat{u}_5(0) & \hat{u}_5(1) \end{bmatrix} \begin{bmatrix} C_{21} \\ C_{22} \end{bmatrix} = \begin{bmatrix} \hat{F}_1(1) \\ \hat{F}_2(1) \\ \hat{F}_3(1) \\ \hat{F}_4(1) \\ \hat{F}_5(1) \end{bmatrix}, \tag{16}$$

where C_{ij}, $i,j = 1, 2$, are unknown constants. In fact, the C_{ij} are the elements of the stiffness matrix we seek; that is, $k_{ij} = C_{ij}$, for $i,j = 1, 2$. These constants may be determined by solving the linear least-squares problems

$$\min_{\mathbf{K}_1} |\mathbf{b}_1 - A\mathbf{K}_1|, \tag{17}$$

and

$$\min_{\mathbf{K}_2} |\mathbf{b}_2 - A\mathbf{K}_2|, \tag{18}$$

where

$$A = \begin{bmatrix} \hat{u}_1(0) & \hat{u}_1(1) \\ \hat{u}_2(0) & \hat{u}_2(1) \\ \hat{u}_3(0) & \hat{u}_3(1) \\ \hat{u}_4(0) & \hat{u}_4(1) \\ \hat{u}_5(0) & \hat{u}_5(1) \end{bmatrix}, \tag{19}$$

$$\mathbf{b}_1 = \begin{bmatrix} \hat{F}_1(0) \\ \hat{F}_2(0) \\ \hat{F}_3(0) \\ \hat{F}_4(0) \\ \hat{F}_5(0) \end{bmatrix}, \quad \mathbf{b}_2 = \begin{bmatrix} \hat{F}_1(1) \\ \hat{F}_2(1) \\ \hat{F}_3(1) \\ \hat{F}_4(1) \\ \hat{F}_5(1) \end{bmatrix}, \tag{20}$$

and

$$\mathbf{K}_1 = \begin{bmatrix} k_{11} \\ k_{12} \end{bmatrix}, \quad \mathbf{K}_2 = \begin{bmatrix} k_{21} \\ k_{22} \end{bmatrix}. \tag{21}$$

In this manner, the stiffness matrix of Eq. (30) is approximated.

We note here that the stiffness matrix, for a single realization $\omega \in \Omega$, is not symmetric ($k_{12} \neq k_{21}$) and, also, $k_{11} \neq k_{22}$. Both of these facts results from the lack of spatial symmetry in perturbation (11), for a given $\omega \in \Omega$, with respect to the midpoint $x = L/2$ of the studied domain. However, in the ensemble setting—when the system is statistically homogenized—the averages satisfy $\langle k_{12} \rangle = \langle k_{21} \rangle$ and $\langle k_{11} \rangle = \langle k_{22} \rangle$.

4. Results, remarks, and conclusions

The first entry, i.e., k_{11}, of these matrices is shown in Figs. 1–3 for the separate cases of inhomogeneity in ρ, E, and A. In each figure plots (a), (b), and (c) correspond, respectively, to g taking values 0.1, 1, and 10. Each particular plot gives k_{11} in the reference (deterministic) case of Section 2, as well as the corresponding ensemble average $\langle k_{11} \rangle$ of the random medium case. The deterministic case is shown as a crisp, black line, while the random case is shown as a grey thicker line, possibly overlapping the first one. Thus, whenever we only see the grey line, there is no difference between the deterministic and the mean of the stochastic problem.

In the numerical studies, we perform a Monte Carlo simulation with 100 realizations and calculate the first moment for each of the cases mentioned above. We also ran a few of the above parameter studies with 1000 realizations. The results were very similar to the ones we got for 100 realizations and we concluded that, for the sake of saving computational time, 100 realizations will suffice.

The results we obtain by letting either ρ or E vary are very similar so we will discuss them together. First, we note that letting these two quantities vary produces a large effect with small to moderate g. By a large effect we mean a strong departure from the reference case at and around the resonant frequencies. Note that the 'scatter interval' increases with increasing frequency. The effects decrease with increasing g but, regardless of the value of g, the effects are most noticeable at higher frequencies. However, variable density has practically no effect for $g = 100.0$ while there is a noticeable effect, especially at higher frequencies, from the variable modulus for the same g.

When A alone is allowed to vary, we see practically no effect for $g = 0.01$ or 0.1. For $g = 1.0$, there is a noticeable effect present for low to mid-range frequencies. However, this effect vanishes at higher frequencies. As g is increased to 10.0, the effect is weaker for lower frequencies but is quite pronounced in the mid to high-frequency range. Finally, when $g = 100.0$, the effect all but vanishes for low frequencies but is still noticeable for higher frequencies.

We ran the parameter studies for the same values of g discussed above but allowed ρ, E, and A all to vary at once. We found trends that should be expected based on the discussion above. In particular, for $g = 0.01$, 0.1, and 1.0, the graphs of the moments for the case when all three parameters vary at once are very similar, qualitatively, to the graphs of the moments for letting density and modulus vary one at a time except that, even at low frequencies, the interval over which the effect is noticeable is larger. For $g = 10.0$, letting all three parameters vary at once leads to graphs for the moments which look very similar to the graphs generated for the case of varying A alone except that, again, the interval over which the effect is noticeable is larger. Also, particularly at higher frequencies, this case also resembles the case of varying E alone (for $g = 10.0$). Finally, for $g = 100.0$, letting all three parameters vary at once again leads to graphs for the moments which look very similar to the graphs generated by letting either E or A vary alone. In particular, the effects are most noticeable at higher frequencies.

5. Spectral finite element for 1-D wave motion in a homogeneous Timoshenko beam

The frequency space equations governing the transverse deflection $v(x,t) = \hat{v}(x)e^{i\gamma t}$ and the transverse shearing deformation w (as measured by the difference $\partial v/\partial x - \phi$, with $\phi(x,t) = \hat{\phi}(x)e^{i\gamma t}$) of a Timoshenko beam, assuming zero external forcing, are well known

$$GA\kappa\left(\frac{d^2\hat{v}}{dx^2} - \frac{d\hat{\phi}}{dx}\right) + \rho A\gamma^2\hat{v} = 0,$$

$$EI\frac{d^2\hat{\phi}}{dx^2} + GA\kappa\left(\frac{d\hat{v}}{dx} - \hat{\phi}\right) + \rho I\gamma^2\hat{\phi} = 0. \tag{22}$$

Here, G is the shear modulus, A is the cross-sectional area, κ is the shape factor of the cross-section, ρ is the mass density, E is the elastic modulus, and I is the cross-sectional-area moment of inertia [6].

The spectral stiffness matrix expresses a connection between the kinematic and the dynamical quantities—i.e., $\{\hat{v}_1, \hat{\phi}_1, \hat{v}_2, \hat{\phi}_2\}$ with $\{\hat{V}_1, \hat{M}_1, \hat{V}_2, \hat{M}_2\}$—at both ends of the beam. The derivation of the spectral stiffness matrix is as follows. For the Timoshenko beam equations (22) along with

the boundary conditions

$$\hat{v}(0) = \hat{v}_1, \quad \hat{\phi}(0) = \hat{\phi}_1,$$
$$\hat{v}(L) = \hat{v}_2, \quad \hat{\phi}(L) = \hat{\phi}_2 \tag{23}$$

set up over a domain of length L, we consider a solution of the form

$$\hat{v}(x) = B_1 R_t \cos k_1 x - B_2 R_t \sin k_1 x + C_1 R_h \cosh k_2 x + C_2 R_h \sinh k_2 x,$$

$$\hat{\phi}(x) = B_1 \sin k_1 x + B_2 \cos k_1 x + C_1 \sinh k_2 x + C_2 \cosh k_2 x, \tag{24}$$

where R_t and R_h are the so-called amplitude ratios and are given by

$$R_t = \frac{GA\kappa k_1}{\rho A\gamma^2 - GA\kappa k_1^2}, \quad R_h = \frac{GA\kappa k_2}{\rho A\gamma^2 + GA\kappa k_2^2}. \tag{25}$$

The boundary conditions of Eqs. (23) specify the constants B_1, B_2, C_1, and C_2 in Eq. (24) and, upon determination of these constants, we may employ Eq. (24) and the relations

$$\hat{V}(x) = -EI\frac{\mathrm{d}^2\hat{\phi}}{\mathrm{d}x^2} - \rho I\omega^2\hat{\phi},$$

$$\hat{M}(x) = EI\frac{\mathrm{d}\hat{\phi}}{\mathrm{d}x} \tag{26}$$

to finish the derivation of the stiffness matrix. However, since this is a long and complicated calculation, we do not reproduce it here. Instead, we refer the reader to Ref. [1] for a complete derivation.

The 11-component of this stiffness matrix is plotted in Figs. 4–8 part (a), in black, as the reference case. The peaks in these figures represent the resonant frequencies of the system with $w = 10^{-2}$ m, $h = 10^{-2}$ m, $E = 27.4$ GPa, $v = 0.0$, and $\rho = 2400$ kg/m^3—this again corresponds to a beam made of concrete. In the next section, we develop a method—analogous to that in Section 3—to determine the departure from this 'crisp' form due to material spatial inhomogeneities.

6. Spectral finite element for 1-D wave motion in an inhomogeneous Timoshenko beam

The frequency space equations of an inhomogeneous Timoshenko beam were given in Eqs. (3). We study a beam with rectangular cross-section having width w, height h, and the Poisson ratio v. For this case, we have the following relations:

$$A = hw, \quad I = \frac{h^3 w}{12}, \quad G = \frac{E}{2(1+v)}. \tag{27}$$

Substituting Eq. (27) into Eqs. (3), we have

$$\frac{\mathrm{d}}{\mathrm{d}x}\left[\frac{Ehw\kappa}{2(1+v)}\left(\frac{\mathrm{d}\hat{v}}{\mathrm{d}x} - \hat{\phi}\right)\right] + \rho hw\gamma^2 v = 0,$$

$$\frac{\mathrm{d}}{\mathrm{d}x}\left[\frac{Eh^3 w}{12}\frac{\mathrm{d}\hat{\phi}}{\mathrm{d}x}\right] + \frac{Ehw\kappa}{2(1+v)}\left(\frac{\mathrm{d}v}{\mathrm{d}x} - \hat{\phi}\right) + \frac{\rho h^3 w}{12}\gamma^2\hat{\phi} = 0. \tag{28}$$

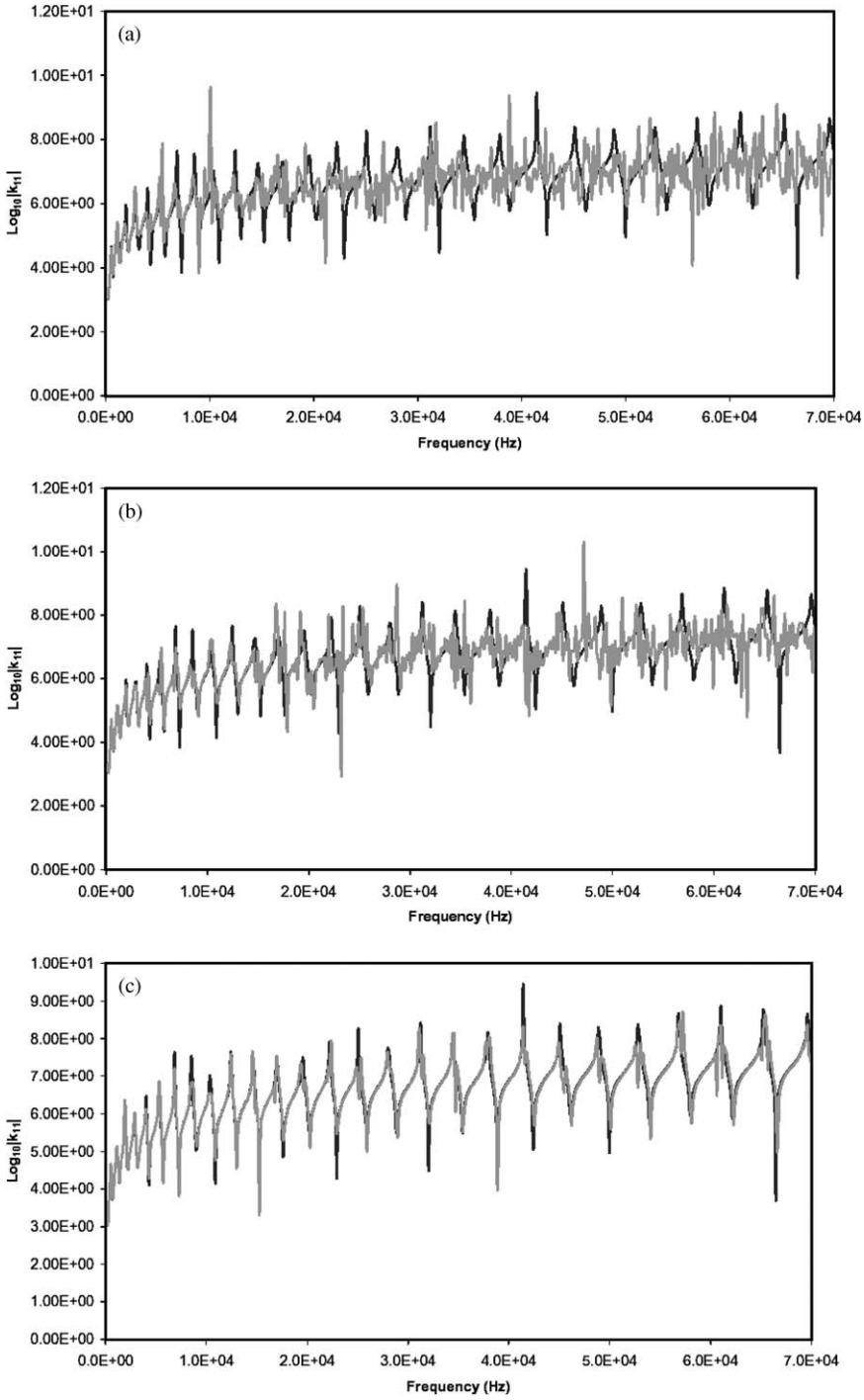

Fig. 4. Timoshenko beam vibrations in the case of random density ρ showing k_{11} (black line) for the reference homogeneous medium and mean $\langle k_{11} \rangle$ (grey line) for the random case with: (a) $g = 0.1$, (b) $g = 1.0$, (c) $g = 10.0$.

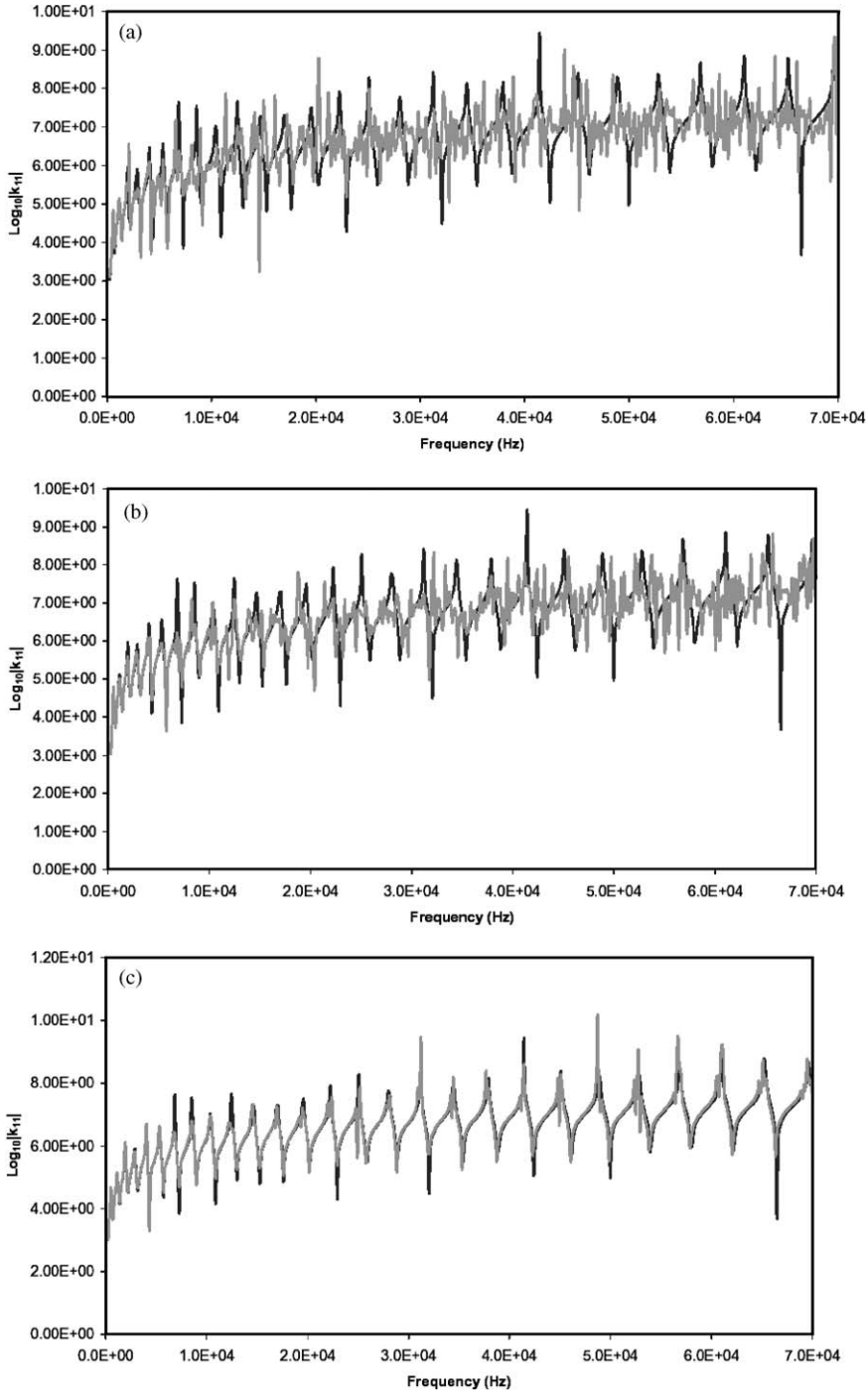

Fig. 5. Timoshenko beam vibrations in the case of random modulus E showing k_{11} (black line) for the reference homogeneous medium and mean $\langle k_{11} \rangle$ (grey line) for the random case with: (a) $g = 0.1$, (b) $g = 1.0$, (c) $g = 10.0$.

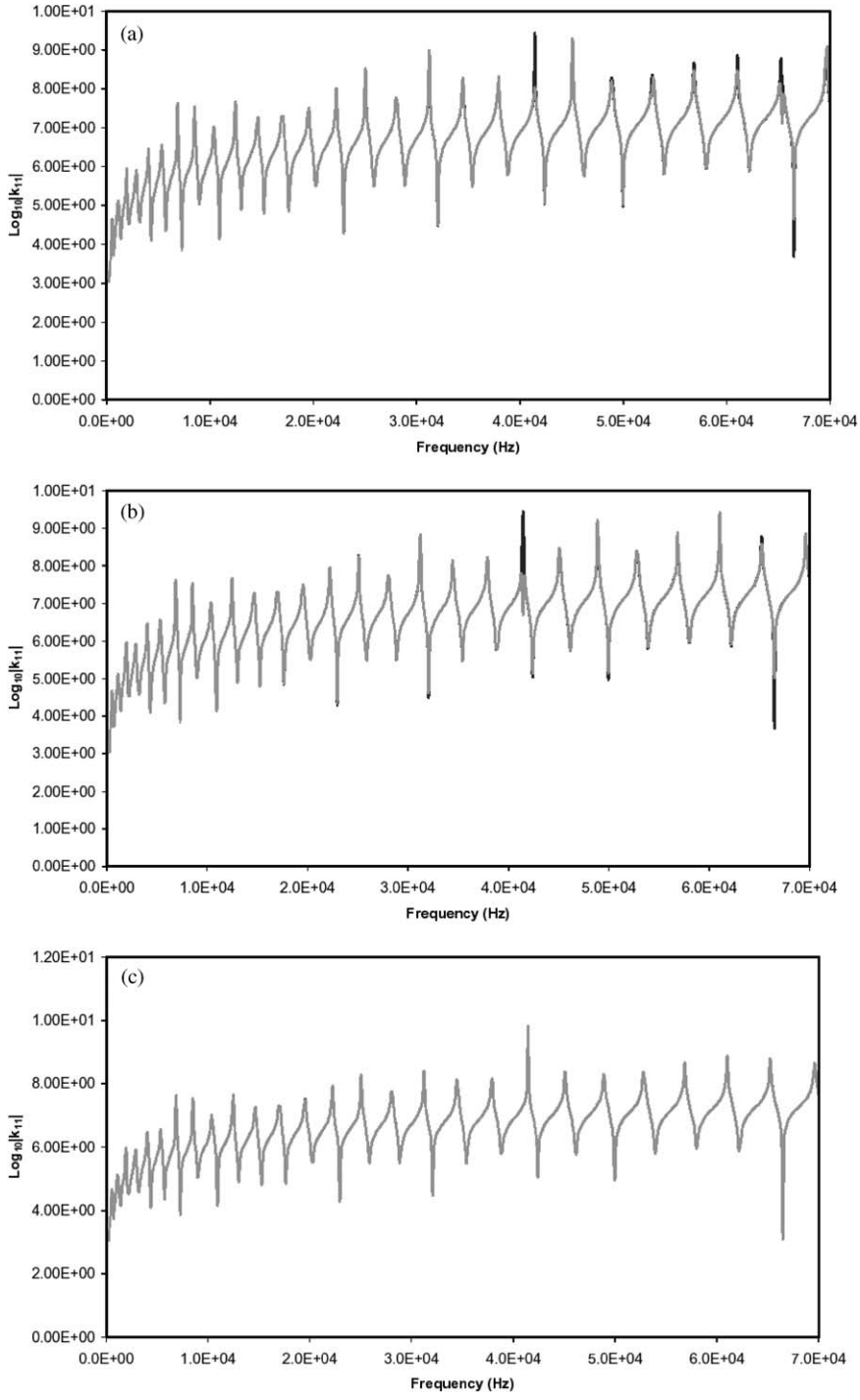

Fig. 6. Timoshenko beam vibrations in the case of random beam the Poisson ratio v showing k_{11} (black line) for the reference homogeneous medium and mean $\langle k_{11} \rangle$ (grey line) for the random case with: (a) $g = 0.1$, (b) $g = 1.0$, (c) $g = 10.0$.

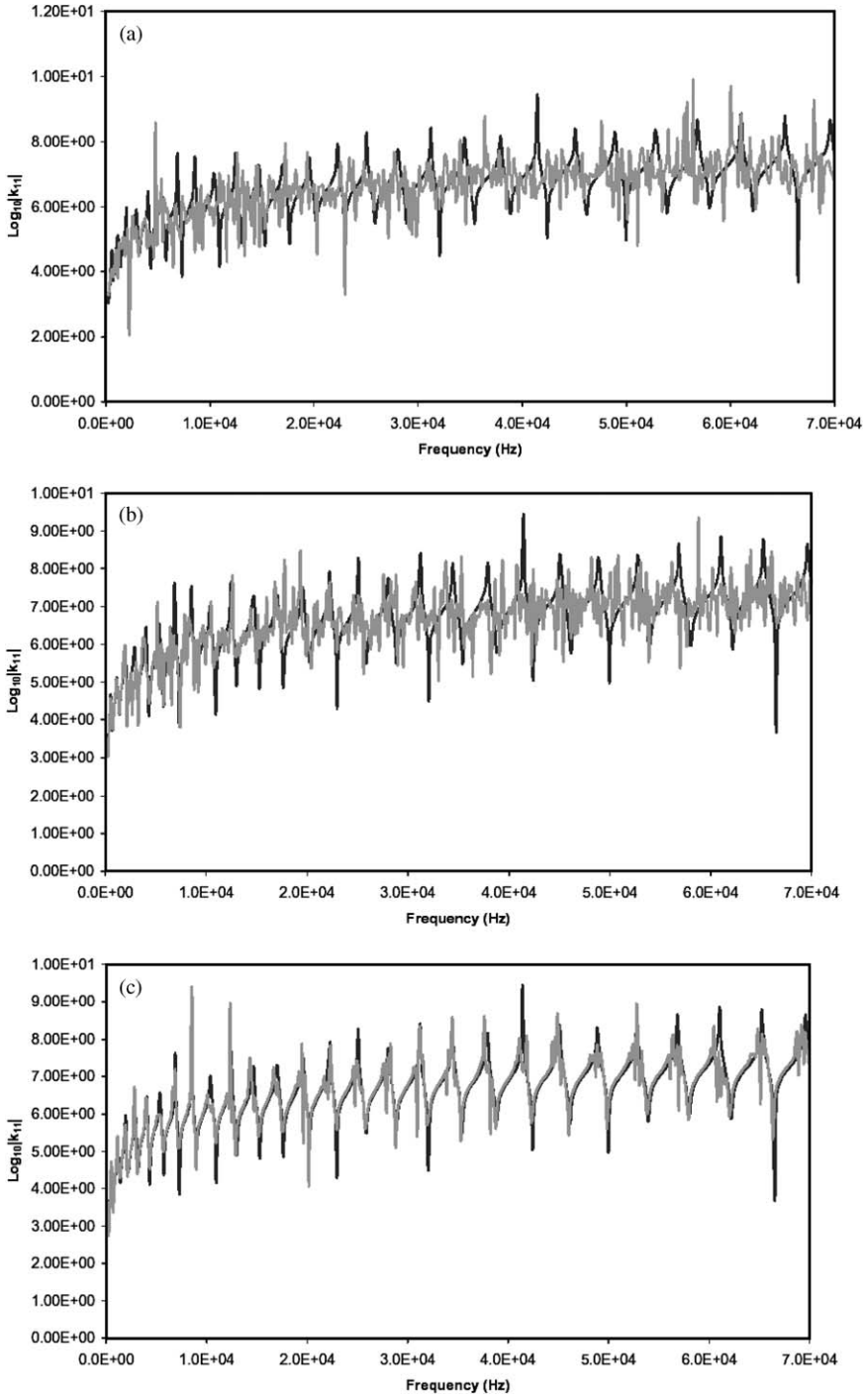

Fig. 7. Timoshenko beam vibrations in the case of random beam height h showing k_{11} (black line) for the reference homogeneous medium and mean $\langle k_{11} \rangle$ (grey line) for the random case with: (a) $g = 0.1$, (b) $g = 1.0$, (c) $g = 10.0$.

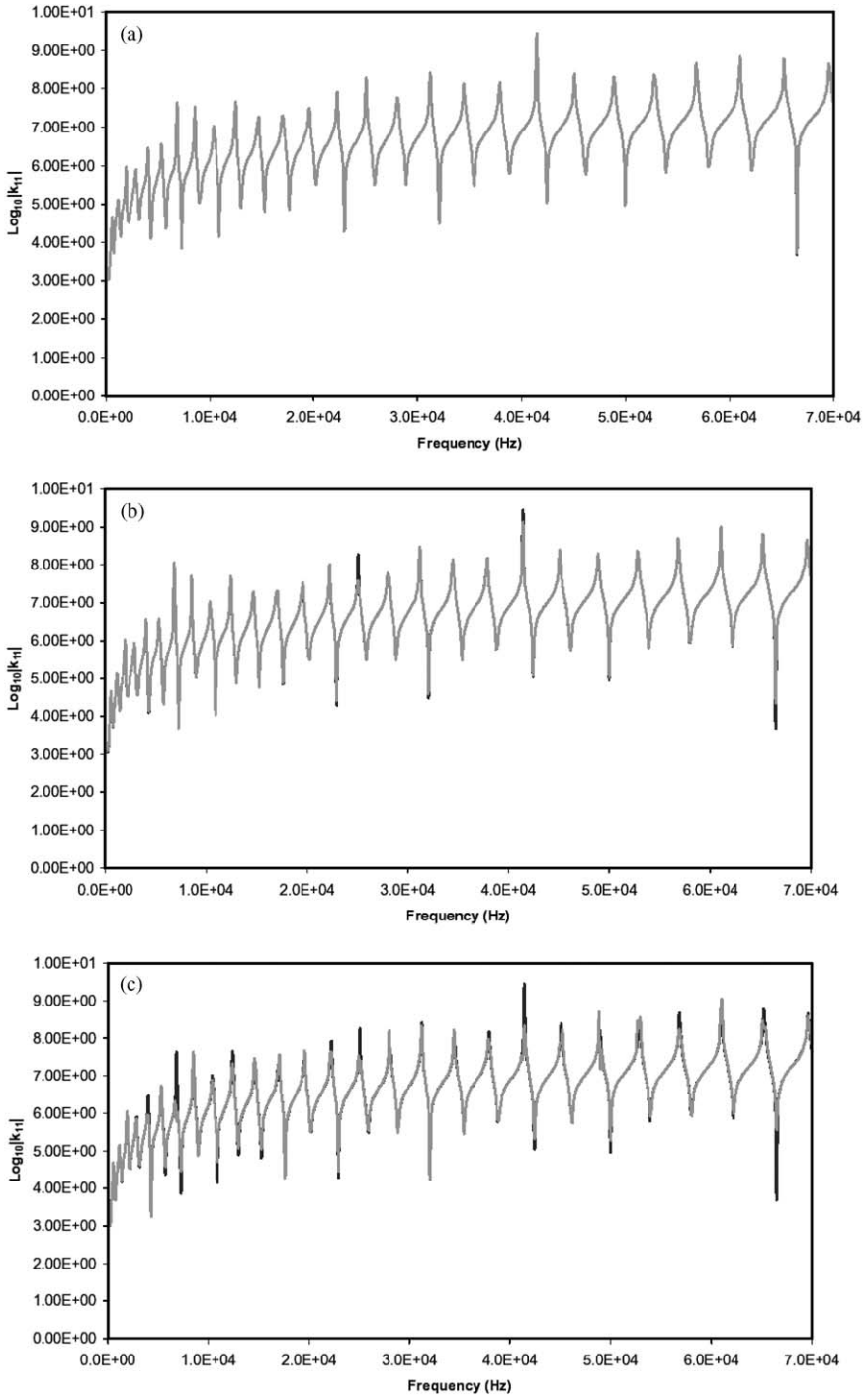

Fig. 8. Timoshenko beam vibrations in the case of random beam width w showing k_{11} (black line) for the reference homogeneous medium and mean $\langle k_{11} \rangle$ (grey line) for the random case with: (a) $g = 0.1$, (b) $g = 1.0$, (c) $g = 10.0$.

We assume the mass density, elastic modulus, cross-sectional height, cross-sectional width, and the Poisson ratio to vary as

$$\rho(x,\omega) = \rho_0\left[1 + \varepsilon_\rho \sum_{i=1}^{10}(a_\rho^{(i)}(\omega)\cos igx + b_\rho^{(i)}(\omega)\sin igx)\right],$$

$$E(x,\omega) = E_0\left[1 + \varepsilon_E \sum_{i=1}^{10}(a_E^{(i)}(\omega)\cos igx + b_E^{(i)}(\omega)\sin igx)\right],$$

$$h(x,\omega) = h_0\left[1 + \varepsilon_h \sum_{i=1}^{10}(a_h^{(i)}(\omega)\cos igx + b_h^{(i)}(\omega)\sin igx)\right],$$

$$w(x,\omega) = w_0\left[1 + \varepsilon_w \sum_{i=1}^{10}(a_w^{(i)}(\omega)\cos igx + b_w^{(i)}(\omega)\sin igx)\right],$$

$$v(x,\omega) = v_0\left[1 + \varepsilon_v \sum_{i=1}^{10}(a_v^{(i)}(\omega)\cos igx + b_v^{(i)}(\omega)\sin igx)\right], \tag{29}$$

where for $i = 1, \ldots, 10$, $a_\rho^{(i)}(\omega), \ldots, b_v^{(i)}(\omega)$ come from a uniform distribution on $[-\frac{1}{2}, \frac{1}{2}]$ and $\omega \in \Omega$. As in the case of longitudinal vibrations of a rod, the purpose of this model is not to approximate some "nice" function, but rather, to have a random process model of band-limited type.

We compute the stiffness matrix; that is, we determine the relation

$$\begin{bmatrix} \hat{V}_1 \\ \hat{M}_1 \\ \hat{V}_2 \\ \hat{M}_2 \end{bmatrix} = \begin{bmatrix} k_{11} & k_{12} & k_{13} & k_{14} \\ k_{21} & k_{22} & k_{23} & k_{24} \\ k_{31} & k_{32} & k_{33} & k_{34} \\ k_{41} & k_{42} & k_{43} & k_{44} \end{bmatrix} \begin{bmatrix} \hat{v}_1 \\ \hat{\phi}_1 \\ \hat{v}_2 \\ \hat{\phi}_2 \end{bmatrix}, \tag{30}$$

in a manner completely analogous to the technique used to compute the spectral stiffness matrix for one-dimensional wave motion in an inhomogeneous rod in the first part of this paper.

7. Results, remarks, and conclusions

For the numerical studies, we first let the parameters ρ, E, h, w, and v vary one at a time for g ranging, by powers of 10, between 10^{-2} and 10^2. With this setup, and having 10 terms in Eqs. (29), we cover a range of frequencies over five orders of magnitude (decades). We perform a Monte Carlo simulation with 100 realizations and calculate the first four moments for each of the cases mentioned above. The first entry, i.e., k_{11}, of these matrices is shown in Figs. 4–8 for the separate cases of inhomogeneity in ρ, E, h, w, and v. In each figure plots (a), (b), and (c) correspond, respectively, to g taking values 0.1, 1, and 10. Each particular plot gives k_{11} in the reference (deterministic) case of Section 5, as well as the corresponding ensemble average $\langle k_{11} \rangle$ of the random medium case. The deterministic case is shown as a crisp, black line, while the random case

is shown as a grey thicker line, possibly overlapping the first one. Thus, whenever we only see the a grey line, there is no difference between the deterministic and the mean of the stochastic problem.

Figs. 1, 2, and 4 show that letting ρ, E, or h vary for $g = 0.1$ and 1.0 has a significant impact on the averaged solution for all but the lowest frequencies. In fact, for $g = 0.01$ (case not shown here), after no more than 10 kHz, the averaged solution $\langle k_{11} \rangle$ resembles random noise. In fact, this disordered behaviour is a result of shifts in the resonant frequencies of the solution for various realizations. The conclusion, then, is that for these low values of g, we can rely on a homogenized solution in only the lowest frequency ranges. The situation improves as we go to higher g values for ρ, E, and h. Already at $g = 1.0$, there is some agreement between the deterministic and the mean at lower frequencies. As we go to $g = 10.0$ and 100.0 (case not shown here), we tend to have an excellent agreement.

As we see from Figs. 6 and 8, the effect of varying w or v for any value of g has almost no effect on the averaged solution at any of the frequency levels we studied. This holds true for $g = 0.01$ or 100.0 as well.

We ran the parameter studies for the same values of g discussed above but allowed all five parameters ρ, E, h, w, and v to vary at once. We found trends analogous to those established above, and in the same vein as those found for vibrations of rods. That is, whenever we are in the range characterized by high sensitivity to randomness of at least one of five parameters, the response is sensitive again or even more disordered than before.

8. Closure

There is a need to gain insight into the dynamics and vibrations of imperfect, structural elements (rods, beams, etc.) as well as large and complex structures made of such components, also in the presence of random properties, see, e.g., Ref. [7]. Recently, progress has been made on elastodynamics of structures described by random fields, see Refs. [8–11] and references therein. The present study should also contribute to an understanding in this area, and especially with respect to axial and flexural vibrations. It has been motivated in the first place by the elastodynamics of concrete and paper, two multiscale materials.

In the context of stochastic mechanics (e.g., Refs. [3,4]), our Eqs. (2) and (3) fall in a general class of problems described by equation

$$\mathscr{L}(\omega)\phi = f, \quad \omega \in \Omega, \tag{31}$$

where $\mathscr{L}(\omega)$ is the differential operator with random field coefficients, ϕ is the sought field, f is the forcing, and Ω is the sample space of elementary outcomes ω (realizations of the random field). Now, the correct average solution $\langle \phi \rangle$ is, in principle, obtained from $\langle \mathscr{L}^{-1} \rangle^{-1} \phi = f$. Almost always, this is different from what would be obtained by straightforward averaging of (1.1): $\langle \mathscr{L} \rangle u = f$. The latter, in fact, is the conventional route of phenomenological deterministic continuum mechanics without regard for microstructural randomness. Black and grey plots in each of our figures correspond to $\langle \mathscr{L} \rangle$ and $\langle \mathscr{L}^{-1} \rangle^{-1}$, respectively.

Introduction of spatial random inhomogeneities into wave mechanics potentially leads to new phenomena, yet their analysis comes at a price of having to solve very difficult governing stochastic equations. In our case these are Eqs. (2) and (3) that are rarely stated in the literature.

At present, there are no satisfactory mathematical methods for their treatment—for instance, the method of Ref. [12] works only in the limits $d \ll \lambda$ or $d \gg \lambda$. We thus opted for a numerical study rather than to attempt any approximate methods whose rigor is uncertain. Our computational method is not original per se, but the parametric investigation is. Of course, depending on a specific model picked from a wide variety of possibilities, the quantitative results will differ. However, the diffusion of resonances away from those of homogeneous rod and beam will always occur. In particular, in the case of rods, the effects of random mass density and elastic modulus—but not of cross-sectional area—are strong. In the case of beams, the effects of random mass density, elastic modulus, and beam's height—but not of the Poisson ratio and beam's width—are strong. Another new aspect, not shown due to the lack of space, is the very high level of second, third and fourth moments of response for a much weaker level of noise in the material.

Acknowledgements

This material is based upon work supported by the National Science Foundation under Grant No. CMS-9713764 and the Canada Research Chairs program.

References

[1] J.F. Doyle, Wave Propagation in Structures: Spectral Analysis Using Fast Discrete Fourier Transforms, Springer, Berlin, 1997.
[2] U. Frisch, Wave propagation in random media, in: A.T. Bharucha-Reid (Ed.), Probabilistic Methods in Applied Mathematics, Vol. 1, Academic Press, New York, 1968, pp. 75–198.
[3] K. Sobczyk, Stochastic Wave Propagation, Elsevier-PWN, Amsterdam-Warsaw, 1985.
[4] D. Jeulin, M. Ostoja-Starzewski (Eds.), Mechanics of Random and Multiscale Microstructures, CISM Courses and Lectures, Vol. 430, Springer, New York, 2001.
[5] J.R. Cash, M.H. Wright, A deferred correction method for nonlinear two-point boundary value problems: implementation and numerical evaluation, SIAM Journal of Scientific and Statistical Computing 12 (1991) 971–989.
[6] K. Graff, Wave Motion in Elastic Solids, Oxford University Press, Oxford, 1975.
[7] L. Jezequel, (Ed.), New Advances in Modal Synthesis of Large Structures: Non-linear Damped and Non-deterministic Cases, A.A. Balkema, Rotterdam, 1997.
[8] C.S. Manohar, S. Adhikari, Dynamic stiffness matrix of randomly parametered beams, Probabilistic Engineering Mechanics 13 (1998) 39–52.
[9] S. Adhikari, C.S. Manohar, Dynamic analysis of framed structures with statistical uncertainties, International Journal of Numerical Methods in Engineering 44 (1999) 1157–1178.
[10] S. Adhikari, C.S. Manohar, Transient dynamics of stochastically parametered beams, American Society of Civil Engineers Journal of Engineering Mechanics 126 (2000) 1131–1140.
[11] C.S. Manohar, C.S. Manohar, Dynamic stiffness method for circular stochastic Timoshenko beams: response variability and reliability analysis, Journal of Sound and Vibration 253 (5) (2002) 1051–1085.
[12] A.K. Belyaev, F. Ziegler, Effective loss factor of heterogeneous elastic solids and fluids, in: M.D.P. Monteiro Marques, J.F. Rodrigues (Eds.), Trends in Applications of Mathematics to Mechanics, Pitman Monographs and Surveys in Pure and Applied Mathematics, Longman, New York, 1994, pp. 3–13.